PROCEEDINGS, 44th Workshop on Geothermal Reservoir Engineering
Stanford University, Stanford, California, February 11-13, 2019
SGP-TR-214

Dimensional Analysis Calculation of Conductive Heat Flux in Lower Geyser Basin, Yellowstone National Park, Wyoming

[1]Cary R. Lindsey, [2]Jerry P. Fairley, and [3]Peter B. Larson

[1]Great Basin Center for Geothermal Energy, University of Nevada Reno, Reno NV 89557

[2]Department of Geological Sciences, University of Idaho, Moscow ID 38844

[3]School of the Environment, Washington State University, Pullman WA 99164

caryl@unr.edu

Keywords: heat flux, conductive, surface, Yellowstone, Nusselt number

ABSTRACT

Conductive heat transfer dominates surface heat flux in non-steaming geothermal areas. Despite this, many scientists have hypothesized that conductive heat flux is negligible when compared to other mechanisms such as advection from surface manifestations. Perhaps this misconception lies in the fact that conductive heat flux is difficult to measure without thermal gradients acquired by costly drilling of gradient wells and is, therefore, not well constrained in many areas. In places such as Yellowstone National Park where drilling is prohibited, it can be virtually impossible to measure directly. By employing techniques of dimensional analysis applied to specific boundary conditions, we constrain the conductive heat flux in the Morning Mist Springs area of Lower Geyser Basin, Yellowstone National Park and show this flux to be non-negligible as compared to advective heat flux from the nearby springs.

1. INTRODUCTION

For decades, scientists have espoused quantification of heat flux in geothermal fields as an important tool for resource characterization and management (Dawson, 1964; Yuhara, 1970; Seward et al., 2018). Increased accuracy of resource parameters such as heat flux can lead to "improved calibration of geothermal reservoir models" (Bromley, et al., 2011), and in areas such as Yellowstone National Park, monitoring of the heat flux is important for recognizing fluctuations in the geothermal system (Vaughan et al., 2012) and for understanding the structural evolution of the caldera (Morgan et al., 1977). Consequently, much work has been done to quantify the heat flux in thermal areas. However, heat transfer mechanisms at play in geothermal system are many and not all are easily measured.

According to Dawson (1964), heat discharge from geothermal systems is comprised of the following mechanisms:

1. heat flow through the soil,
2. heat loss from water surfaces,
3. fumaroles,
4. discharge from geysers and springs, and
5. seepage to nearby water bodies.

In a more recent inventory, Sorey and Colvard (1994) proffer the following formula to capture heat flux:

$$H_{tot} = H_{fum} + H_{adv} + H_{evap} + H_{rad} + H_{cond} + H_{gr}, \quad (1)$$

where H_{fum} is the differential advective heat loss in fumaroles, H_{adv} is advective heat loss in streams and springs, H_{evap} is the evaporative heat loss from water surfaces, H_{rad} is the radiative heat loss from water surfaces, H_{cond} is conductive heat loss from water surfaces, and H_{gr} is the heat flow from bare ground by convection, evaporation, and conduction. Despite differences in nomenclature, both explanations provide some insight into the complexity of heat transfer in geothermal fields. To add to this complexity, each heat transfer mechanism requires different measurement techniques. Calorimeters have been employed to measure the advective heat flux in steaming areas (e.g., Benseman, 1959; Dawson, 1964; White, 1969; Bromley and Hochstein, 2005); chloride mass balance of fluids leaving the caldera has been used in Yellowstone National Park (e.g., Fournier, 1975; Hurwitz et al., 2007; Friedman and Norton, 2007); ASTER thermal infrared data has been used in various locations to measure radiative heat flux (e.g., Vaughan et al., 2012); shallow subsurface temperature readings from 0.15 to 2.0 meters have been taken in geothermal areas across the globe (e.g., Fairley and Hinds, 2004; Rissman et al., 2012; Hurwitz et al., 2012; Coolbaugh et al., 2014); and others have employed multiple techniques (e.g., Seward et al., 2018). The large body of existing work clearly demonstrates the importance of this parameter; however, each of the aforementioned methods has inaccuracies or weaknesses, and these are often related to the estimation of conductive heat flux.

In the present work, we address the conductive component of H_{gr}. To do this, we apply a type three boundary condition, also known as a Robin boundary or conductive/advective boundary. At this boundary, the advective and conductive heat fluxes must be equal; therefore, solving for one provides the other. As mentioned previously, the conductive flux is notoriously difficult to obtain and for this reason, we solve for the advective flux. We accomplish this by calculating the Nusselt number, the dimensionless coefficient of convective heat transfer at the air/surface boundary, through dimensional analysis. Here, we present the calculation of the Nusselt number and use it to calculate the advective and conductive heat fluxes at the land surface. In addition, we compare the estimated conductive and advective heat fluxes in a geothermal discharge area in Yellowstone National Park. Although this is a common approach to estimating heat transfer in, for example, mechanical engineering, we are unaware of any previous applications of the method in the geosciences.

2. SITE DESCRIPTION

The study area is located in the Morning Mist Springs area of Lower Geyser Basin in Yellowstone National Park. Lower Geyser Basin is the largest hydrothermal area in Yellowstone National Park and discharges more hot water than any other area of the Yellowstone caldera (Marler, 1964). The basin is home to hundreds of thermal features including geysers, hot springs, and mud pots, the most common being neutral chloride-rich springs. Surficial sediments in the Lower Geyser Basin consist of glacial and alluvial sediments, as well as deposits of precipitates from thermal discharge (Muffler et al., 1982). Rhyolite plateaus ranging from 120 to 300 meters high surround the basin with ages of the flows ranging from 120,000 to 600,000 years (Muffler et al, 1971).

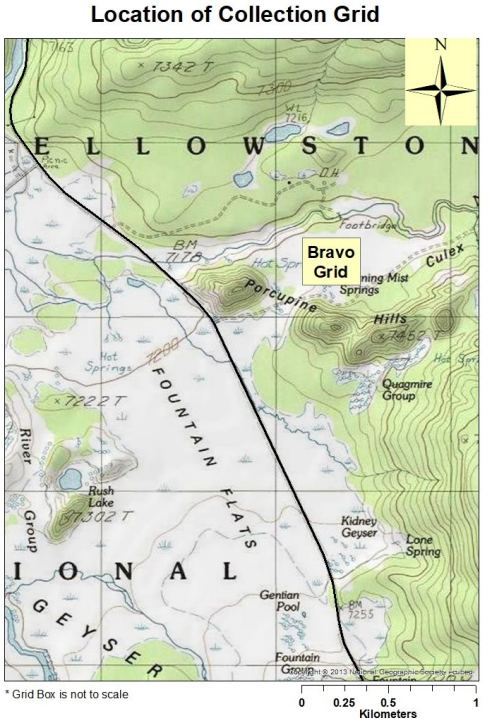

Figure 1: Map of Bravo grid location.

The collection grid, hereafter referred to as Bravo grid, is located about 0.5 kilometers off Grand Loop Road just off the west end of the Mary Mountain Trailhead, south of Nez Perce Creek and east of Porcupine Hill (Figure 1). The area is a flat, grassy plain dotted with thermal features (Figure 2). The area contains one major spring, identified by the Yellowstone Research Coordination Network as LCBNN159 (Rodman and Guiles, 2008) and by Lubenow et al. (2016) as Bravo, with a hand full of subsidiary springs. Deposits of sinter form near the springs and lightly colored silt fills the flat, marshy areas. Sands and gravels from the Pinedale Glaciation surround the area (Muffler et al., 1982).

Figure 2: View of Bravo field area from Porcupine Hill facing east.

3. METHODS

3.1 Ground Temperature Measurements

Shallow subsurface temperatures were collected on a 72 x 72 meter grid at 3 meter intervals. We used 20 centimeter Omega Rugged Penetration Thermocouple Probes (K-type) with a "T" handle connected to Fluke 51 II single input digital thermometers with a reported accuracy of ±0.05% + .03 °C.

For field areas in which spatial correlation of the measured variable (i.e. temperature) is likely, performing a thorough geostatistical analysis allows for identification of the spatial correlation structure within the field. Including correlation structure in interpolation leads to predicted values that better reflect the true distribution of temperatures in the system. The statistical analysis involves computing the square of the difference in temperature between pairs of collected ground temperatures and plotting them as a function of their separation distance. The result is an experimental variogram, which can then be fit with a model variogram to discern the necessary parameters of correlation. Several model variograms exist, including spherical, Gaussian, linear, and power, and these models (or their linear combinations) are matched to the shape of the experimental variogram to determine the best representation of the underlying generating process.

Once the appropriate model is selected, the model parameters must be estimated. These parameters generally consist of the model sill (for stationary variables), the range, and the nugget. The sill represents the variance in the data; the range, the extent of spatial correlation; and the nugget, errors at small scales (usually a distances smaller than the sampling resolution). Once these parameters are defined, the resulting model of spatial correlation can be employed to estimate the values of unsampled points (i.e., kriging), for simulating possible spatial distributions, or for other geostatistical analyses.

3.3 Nusselt Calculation

A Robin boundary, or an advection/conduction boundary, is defined by the following equation (Fairley, 2016):

$$-k_T \frac{dT}{dz}(z=0,y,t) = h[T(z=0,y,t) - T_\infty], \tag{2}$$

Where the left-hand side represents conductive heat transfer at the boundary and the right-hand side represents advective heat transfer at the boundary. For the homogeneous equation, advective flux and conductive flux must balance across the boundary; that is, the conductive heat flux from the subsurface is equal to the flux of heat transported away from the boundary by fluid flow (the atmosphere). As a result, if one of the two fluxes is known, the other is as well. The left-hand side of the equation includes the geothermal gradient, which is desired, but poorly constrained. For this reason, we concentrate on estimating the right-hand side of the equation. Air temperatures and ground temperatures were collected in the field leaving only the coefficient of convective heat transfer, h, unknown. This quantity is typically estimated from dimensional analysis using the average Nusselt number.

The Nusselt number is dimensionless heat transfer parameter between a surface and a fluid, in this case, the air. The Nusselt number is related to h by the following equation (Incropera et al., 2007):

$$Nu_L = \frac{hL}{k}, \tag{3}$$

where h is the convective heat transfer coefficient, L is the characteristic length, and k is the thermal conductivity of the air. Rearranging this formula, we solve for h:

$$h = \frac{Nu_L k}{L}. \tag{4}$$

The Nusselt number can also be written as a function of the Rayleigh and/or Prandtl numbers, or other dimensionless parameters of heat transfer. The Rayleigh number is typically thought of as defining the flow regime (i.e., laminar or turbulent), but is more accurately described as the ratio of inertial to viscous forces of a fluid. The Prandtl number is the ratio of viscous and thermal diffusivity of a fluid. Nusselt number correlations are empirically derived based upon geometry and flow regime. Common geometries are vertical plates, cylinders, and horizontal plates. For this study, we assume a horizontal plate geometry of length-scale L, with L being the distance of spatial correlation as defined by the range of the variogram. For a horizontal plate with a Rayleigh number between 10^7 and 10^{11} (which will be shown to be reasonable in the following calculations), the Nusselt number is only a function of the Rayleigh number and the empirically derived correlation equation for the average Nusselt number is (Incropera et al., 2007):

$$Nu_L = 0.15 Ra_L^{\frac{1}{3}}. \tag{5}$$

It should be noted that we calculate the Nusselt number, Nu_L. The average Nusselt evaluates the field as one body whereas the local Nusselt number, Nu_x, uses the distance from the plate edge to the point of interest for the calculation:

$$Nu_x = \frac{hx}{k}, \tag{6}$$

where h is the local (point) coefficient of convective heat transfer, x is the distance from the plate edge to some point of interest, and k is the thermal conductivity of the fluid.

The following variables are required to calculate Nu_L using the method outlined in this paper:

- x coordinate on grid;
- y coordinate on grid;
- temperature (°C) at 20 cm depth, $T_{(z=20)}$, for all x and y pairs;
- air temperature, T_∞ (°C), for all times of $T_{(z=20)}$ measurements (for our study, air temperatures were recorded at 45-second intervals over a 7-day period with a Fluke beaded thermocouple with a range of -40 to 260 °C and a reported accuracy of ±1.1 °C);
- film temperature, T_f(°C), for all x and y pairs, calculated using the following formula:

$$T_f = \frac{T_{(z=20)} + T_\infty}{2}; \tag{7}$$

- thermal conductivity of fluid (k_{fluid} in W/mK), based upon average air temperature from Incropera et al. (2007);
- fluid density (ρ_{fluid} in kg/m^3), calculated using the formula for dry air density:

$$\rho = \frac{p}{R_{sp} T}, \tag{8}$$

where p is air pressure in Pascals, R_{sp} is the specific gas constant for dry air, 287.058 J/kgK, and T is temperature in Kelvins;

- dynamic viscosity of fluid in kg/ms (μ) obtained from linear regression of tabulated data from dynamic viscosity (Incropera et al., 2007);
- specific heat of fluid (Cp) in J/kgK , obtained from linear regression of tabulated data from specific heat (Incropera et al., 2007);
- kinematic viscosity of fluid in m^2/s (ν), calculated from the following equation:

$$\nu = \frac{\mu}{\rho}; \tag{9}$$

- thermal diffusivity of fluid (α_{fluid}), in m^2/s calculated using the following equation:

$$\alpha = \frac{k}{\rho C_p}; \tag{10}$$

- thermal expansion of fluid (β) in 1/K, calculated using the following equation:

$$\beta = \frac{1}{T_{z=20}}, \tag{11}$$

where $T_{(z=20)}$ is in Kelvins;

- the Prandtl number (Pr), calculated using the following equation:

$$Pr = \frac{C_p \mu}{k}; \tag{12}$$

- characteristic length in meters (L), given by the formula:

$$L = \frac{A_s}{P}, \tag{13}$$

where A_s is the area of the horizontal plate and P is the perimeter;

- the Grashof number (Gr) calculated using the following formula:

$$Gr = \frac{g\beta(T_{(x=L)} - T_\infty}{\nu^2}; \tag{14}$$

and finally,

- the Rayleigh number (Ra) given as:

$$Ra = GrPr. \tag{15}$$

The equations given above, in this order, end with the calculation of the Rayleigh number which is then used in Equation (5) to solve for the average Nusselt number. In turn, this number is used to solve for the coefficient of convective heat flux in Equation 4. Finally, plugging the values for h into Equation (2), we solve the right-hand side of the equation and in doing so obtain a value for the left-hand side, which allows calculation of the conductive heat flux at each (x,y) point.

4. RESULTS

4.1 Ground Temperature Measurements

Over 600 shallow-subsurface temperatures were recorded over the 72 meter x 72 meter field area. As outlined in the methods, the spatial correlation structure of the temperatures was determined using geostatistical analysis. The plotted variogram can be seen in Figure 3. We fit the experimental variogram using a spherical model, with a nugget of 0.25, a sill of 14, and a range of 27 meters. The formula for the spherical model can be seen in Equation 16. Using the model of spatial correlation structure, we employed ordinary kriging to estimate values at unsampled locations of the study plot and generated a high-resolution contour map of temperatures (Figure 4). The analysis was done in R (R Core Ream, 2014).

$$\gamma(h) = \begin{cases} c\left[1.5\left(\frac{h}{a}\right) - 0.5\left(\frac{h}{a}\right)\right], & h \le \alpha \\ c, & h > \alpha. \end{cases} \quad (16)$$

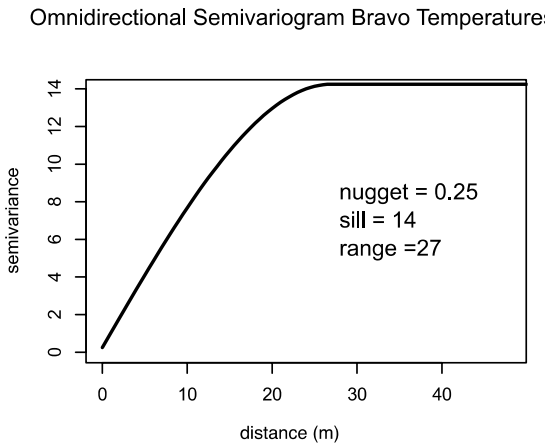

Figure 3: Variogram of shallow subsurface temperatures from Bravo grid.

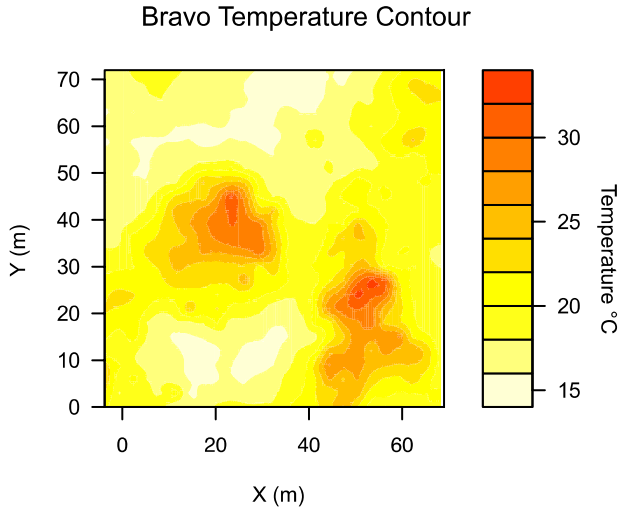

Figure 4: Kriged shallow subsurface temperatures at Bravo grid.

4.3 Nusselt Calculation

Once the Nusselt number calculation was applied to the temperature data, it was discovered that some Nusselt values were negative (i.e. the air temperature was hotter than the ground temperature) and could not be used to calculate the conductive heat flux. A negative flux in this case is a transient condition, representing *into* the ground. For this study, we focused on positive fluxes (flux *from* the geothermal system), so negative flux values were not considered. Further examination may show that there is some dampening of the flux due to this and we hope to address that in subsequent investigations.

As with the temperature measurements, it was necessary to determine any spatial correlation within the data. The same methods applied to the temperature data were applied to the flux values. Again, the best-fit model was a spherical model but the parameters were quite different, with a nugget of 2.5, a sill of 13, and a range of 12 meters (Figure 5). The parameters from the model variogram were applied to the interpolation of heat flux values with a spacing of 0.5 meters. The resulting contour map of predicted heat flux values is presented in Figure 6.

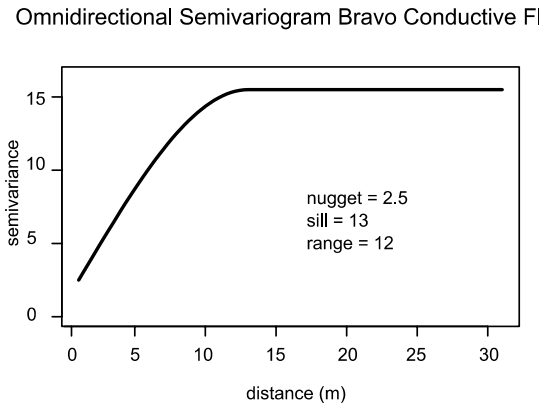

Figure 5: Variogram of conductive heat flux at Bravo grid.

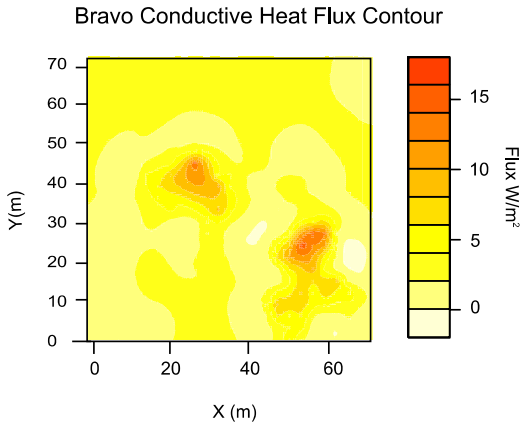

Figure 6: Contour plot of heat flux at Bravo field location.

The predicted values were summed and multiplied by the areas of each square of the contour grid as given in the following formula:

$$\sum_{n=1}^{\infty} q_i A = P, \tag{17}$$

where q is the conductive heat flux in W/m^2, A is the area of each grid block on the contour map in m^2, and P is the power in watts generated by the conductive heat flux across the 72 x 72 meter grid around Bravo hot spring. Performing the indicated operations yields a total output of approximately 13,000 watts. The average heat flux across the area is 2.39 W/m^2 with a maximum flux of 16.94 W/m^2.

5. DISCUSSION

Evaluation of the power output by conductive heat flux near Bravo hot springs, as it compares to the advective heat flux from the hot spring itself, indicates that conductive heat flux is not a trivial portion of the total heat output. McMillan et al. (2018) employed a deuterium doping method to calculate the volume and subsequent advective output of Bravo hot spring and suggested an output of 18,900 watts. Combined with the conductive output calculated here, that is a total of 31,900 watts, 41% of which is the product of conductive heat flux. That is an average of approximately 5.5 W/m^2 in the 5,184 m^2 field site.

In the Vaughan et al. (2012) study, researchers used thermal infrared data to capture radiative heat flux in the caldera. The values proffered by Vaughan for the Morning Mist Springs area are consistent with the minimum and maximum values calculated in this study. Admittedly, the radiative method misses some modes of heat loss such as advection at the water surface and while it is not expected that the conductive heat flux and the radiative heat flux will be the same, it is encouraging to note that the values are of the same order of magnitude and range.

As this applies to Yellowstone caldera, these findings may suggest that previous studies have underestimated heat flux from the caldera. The average heat flux in Yellowstone is thought to be approximately 2 W/m^2, and can be as high as 150+ W/m^2. The Morning Mist Springs field site is not one of the higher heat flux areas of the park, for example, in contrast to Norris Geyser Basin or vapor-dominated areas in the eastern caldera. In fact, according to work done by Vaughan et al. (2012), the area is in the lower one-third of radiative heat flux values in the caldera. These findings suggest that a re-evaluation of direct heat flux estimates for the caldera may be in order.

6. CONCLUSION

In this study, we have presented a dimensional analysis method for calculating conductive heat flux from the ground in geothermal systems. The necessary data for the analysis were collected with minimal invasion and a relatively modest budget. The results align well with the work of others in the Yellowstone Caldera (e.g., Vaughan et al., 2012), but make clear that more work is needed to obtain a true heat budget in the caldera. We emphasize that any one method alone, including the one presented here, cannot capture all the nuances of such a complex system.

There are several ways in which the results of this study could be improved and expanded upon; in particular:

- A more thorough analysis of sensitivity and errors of the calculations is needed,
- multi-directional (i.e., anisotropic) spatial correlation analysis of the temperature and flux data may be valuable; and
- comparison of calculations from other sites (currently we have temperature data from two other locations in the Yellowstone Caldera) and potentially against known (laboratory) data.

REFERENCES

Anderson, T.R. and Fairley, J.P.: Relating Permeability to the Structural Setting of a Fault-Controlled Hydrothermal System in Southeast Oregon, USA, *Journal of Geophysical Research Solid Earth,* 113 (B5), (2008), B05402.

Benseman, R.F., The Calorimetry of Steaming Ground in Thermal Areas, *Journal of Geophysical Research*, 64 (1), (1959), 123-126.

Bromley, C.J. and Hochstein, M.P.: Hat Discharge from Steaming Ground at Karapiti (Wairakei), New Zealand, *Proceedings*, World Geothermal Congress, Antayla, Turkey (2005).

Bromley, C.J. van Manen, S.M., and Mannington, W.: Heat Flux from Steaming Ground; Reducing Uncertainties. *Proceedings*, Thirty-Sixth Workshop on Geothermal Reservoir Engineering, Stanford University, Stanford, CA (2011).

Coolbaugh, M., Sladek, C., Zehner, R., and Kratt, C.: Shallow Temperature Surveys for Geothermal Exploration in the Great Basin, USA, and Estimation of Shallow Aquifer Heat Loss, *Transactions*, Geothermal Resources Council Annual Meeting, (2014), 115-122.

Dawson, G.B.: The Nature and Assessment of Heat Flow from Hydrothermal Areas, *New Zealand Journal of Geology and Geophysics*, 7 (1), (1964), 155-171.

Fairley, J.P., Heffner, J., and Hinds, J.: Geostatistical Evaluation of Permeability in an Active Fault Zone, *Geophysical Research Letters,* 20 (18), (2003), 5.1-5.4.

Fairley, J.P. and Hinds, J.H.: Rapid Transport Pathways for Geothermal Fluids in an Active Great Basin Fault Zone, Geology, 32(9), 825-828.

Fairley, J.P. (2016). *Models and Modeling: An Introduction for Earth and Environmental Scientists*. Hoboken, NJ: John Wiley and Sons.

Fournier, R.O., White, D.E., and Truesdell, A.H.: Convective Heat Flow in Yellowstone National Park, *Proceedings*, U.N. Symposium on the Development and Use of Geothermal Resources, San Francisco, CA (1975).

Friedman, I. and Norton, D.R.: Is Yellowstone Losing Its Steam? – Chloride Flux Out of Yellowstone National Park, LA Morgan (Ed.), *Integrated Geoscience Studies in the Greater Yellowstone Area: Volcanic, Hydrothermal and Tectonic Processes in the Yellowstone Geoecosystem*, U.S. Geological Survey Professional Paper, (1717), (2007), 275-297

Hurwitz, S., Lowenstern, J.B., Heasler, H.: Spatial and Temporal Geochemical Trends in the Hydrothermal System of Yellowstone National Park: Inferences from River Solute Fluxes, *Journal of Volcanology and Geothermal Research*, 162, (2007), 149-171.

Hurwitz, S., Harris, R.N., Werner, C.A., and Murphy, F.: Heat Flow in Vapor Dominated Areas of the Yellowstone Plateau Volcanic Field: Implications for the Thermal Budget of the Yellowstone Caldera, Journal of Geophysical Research, 117 (B10207), (2012).

Incropera, F.P., Dewitt, D.P., Bergman, T.L., and Lavine, A.S. (2007). *Fundamentals of Heat and Mass Transfer, Sixth Edition*. Hoboken, NJ: John Wiley and Sons.

Lubenow, B.L., Fairley, J.P., Lindsey, C.R., and Larson, P.B.: Influences on Shallow Ground Temperatures in High Flux Thermal Systems, *Journal of Volcanology and Geothermal Research*, 323, (2016), 53-61.

Marler, G.D. (1964). *Studies of Geysers and Hot Springs along the Firehole River*. Yellowstone Library and Museum Association.

McMillan, N., Larson, P., Fairley, J., Mulvaney-Norris, J., and Lindsey, C.: Direct Measurement of Advective Heat Flux from Several Yellowstone Hot Springs, Wyoming, USA, *Geosphere*, 14 (4), 1860-1874.

Morgan, P., Blackwell, D., Spafford, R. and Smith, R.: Heat Flow Measurements in Yellowstone Lake and the Thermal Structure of the Yellowstone Caldera, Journal of Geophysical Research, 82 (26), (1977), 3719-3732.

Muffler, L.J.P., White, D.E., and Truesdell, A.H.: Hydrothermal Explosion Craters in Yellowstone National Park, *Geological Society of America Bulletin*, 82, (1971), 723-740.

Muffler, L.J.P., White, D.E., Truesdell, A.H., and Fournier, R.: Geologic Map of Lower Geyser Basin, Yellowstone National Park, Wyoming. Miscellaneous Investigations Series Map I-1373, United Sates Geological Survey, (1982).

Rissman, C., Christensen, B., Werner, C., Leybourne, M., Cole, J., and Gravley, D.: Surface heat Flow and CO_2 Emissions Within the Ohaaki Hydrothermal Field, Taupo Volcanic Zone, New Zealand, *Applied Geochemistry,* 27(1), (2012), 223-239.

R Development Core Team: R: A Language and Environment for Statistical Computing, R Foundation for Statistical Computing, Vienna, Austria (ISBN 3-900051-07-0) (2008).

Rodman, A., Guiles, C.: Greater Yellowstone Science Learning Center and the Yellowstone Thermal Inventory. In: Inskeep, W., Peters, J. (Eds.), *Geothermal Biology and Geochemistry in Yellowstone National Park*, NSF Research Coordination Network and Montana State University Thermal Biology Institute Workshop.

Seward, A., Ashraf, S., Reeves, R., and Bromley, C.: Improved Environmental Monitoring of Surface Geothermal Features Through Comparisons of Thermal Infrared, Satellite Remote Sensing, and Terrestrial Calorimetry, Geothermics, (73), (2018), 60-73.

Sorey, M.L. and Colvard, E.M.: Measurements of heat and Mass Flow from Thermal Areas in Lassen Volcanic National Park, CA, 1984-93, U.S. Geological Survey, USGS Earth Science Information Center, Open-File Reports Section. (1994).

Vaughan, R.G., Keszthelyi, L.P., Lowenstern, J.B., Jaworowski, C., and Heasler, H.: Use of ASTER and MODIS Thermal Infrared Data to Quantify Heat Flow and Hydrothermal Change at Yellowstone National Park, *Journal of Volcanology and Geothermal Research*, (233-234), (2012), 72-89.

White, D.E.: Rapid Heat-Flow Surveying of Geothermal Areas, Utilizing Individual Snowfalls as Calorimeters, *Journal of Geophysical Research*, 74 (22), (1969), 5191-5201.

Yuhara, K.: Heat Transfer Measurement in a Geothermal Area, *Tectonophysics*, 10 (1), 1970, 19-30.